Transient Response of a Thermoelectric Generator to Load Steps Under Constant Heat Flux

Marcos Compadre Torrecilla,a,b, Andrea Montecuccoa,c, Jonathan Sivitera,c, Andrew Strainb, Andrew Knoxa,c*

aSchool of Engineering, University of Glasgow, G12 8LT, UK
bClyde Space Ltd., 5B Skypark 5, 45 Finnieston Street, G3 8JU
cThermoelectric Conversion Systems Ltd.
**Corresponding Author: m.compadre.1@research.gla.ac.uk*

Keywords: Thermoelectric, MPPT, Constant Heat, Transient Response, Seebeck, Peltier

Abstract
Most waste heat recovery applications involve a heat source that provides a limited heat flux that can be converted into electricity by a thermoelectric generator (TEG). When a TEG is used under limited or constant heat flux conditions the temperature difference across the device cannot be considered constant and will change depending on the electrical current generated by the TEG. This phenomenon is induced by the Peltier effect, which works against power generation and deviates the optimum operating point from the commonly known maximum power point (MPP). This point, dictated by the *maximum power transfer theorem,* is achieved when the source equivalent series resistance and the load resistance are equal, in conditions of constant temperature difference. Hence maximum power point tracking (MPPT) algorithms that regulate the TEG at half of the instantaneous open-circuit voltage are optimized only for applications where the TEG operates under constant temperature difference but are not ideal for constant heat flux conditions. Hill climbing MPPT methods, e.g., perturb-and-observe (P&O) or incremental conductance (IC), can reach the MPP more accurately if the sampling time is extended to the thermal time constant of the system.
This article presents an analysis of the transient electrical and thermal response of a TEG to a load change. This investigation results fundamental to the design of MPPT algorithms such P&O or IC for TEGs operating under constant heat flux. A step-up (boost) dc-dc converter controlled by P&O is used to demonstrate the effects of the sampling time over of the transient response and hence the tracking performance of the MPPT algorithm.

1. Introduction

Thermoelectric generators (TEGs) are solid-state devices that convert thermal energy into electrical energy exploiting the Seebeck effect. TEGs do not have any moving parts; they are small, compact in size and very robust. The use of TEGs is not widely extended due to their low efficiency, around 5%. Thermoelectric technology gained more commercial success in cooling applications where thermoelectric devices are used as heat pumps [1].
TEGs have been used in the past in applications where only thermal energy was available *e.g.*, in space or remote applications, as in the *Voyager* mission. More recently researchers have proposed applications of TEGs to generate electricity from waste heat [2] that otherwise would be lost in the environment. Some examples are energy generation from a combustion chamber [3], biomass cooking stove [4], wood burning stove [5], [6] or gas stove [7], [8]. Other applications can be found in the automotive sector where the heat sources are the exhaust [9], [10], [11] or a catalytic combustor [12]. In these applications proper thermal management is required and some applications using heat pipes have been developed [13]. TEGs can also be connected in series and in parallel to adjust the overall output voltage and current of the TEG module [14]. In most of the referenced applications the heat source can provide only a limited amount of thermal energy. The temperature gradient developing across the TEG system depends on the thermal resistance of the heat exchangers and the TEG devices.
It is commonly accepted in literature [15], [16] that the MPP of a TEG operating under constant temperature difference can be found from the *maximum power transfer theorem* which states that the generated power is maximised when the external electrical load is matched to the TEG's internal resistance, *i.e.* $R_{source} = R_{load}$. Under these conditions the load voltage settles at half of the open-circuit voltage, *i.e.* $V_{load} = 0.5 \cdot V_{oc}$ or, defining a new parameter, $\beta = V_{load}/V_{oc} = 0.5$. However, in real applications the temperature gradient across the TEGs is never constant. It varies with the thermal power available and with the effective thermal resistance of the TEG devices. In fact, the heat flux through the TEG from the hot to the cold side changes with the load current generated by the TEG

according to the Peltier effect, considered parasitic in power generation. This effectively means that the thermal resistance of the TEG device varies with the electrical current that it generates. Eq. (1) represents the sum of powers at the hot side of a TEG in power generation mode and thermal steady-state conditions.

$$Q_H = K\Delta T + \alpha T_H I - \frac{1}{2}RI^2 \tag{1}$$

Where Q_H is the heat flux absorbed by the TEG at the hot side, $K\Delta T$ is the thermal conduction term, $\alpha T_H I$ is the heat transfer from the hot side due to the Peltier effect and $0.5 \cdot RI^2$ is the heat flowing back to the hot side due to internal Joule heating. This equation is obtained solving the one-dimensional heat conduction equation for thermoelectric generators [17], [18]. The Thomson effect, which describes the variation of the Seebeck coefficient α with average temperature is here neglected due to its small contribution compared to the other terms [19].
Substituting $T_H = T_C + \Delta T$, being ΔT the temperature across the TEG, into Eq.(1) we obtain Eq.(2).

$$\Delta T = \frac{Q_H + \frac{1}{2}RI^2 - \alpha T_C I}{K + \alpha I} \tag{2}$$

As shown in Eq (2), there is an amount of heat that flows from the hot to the cold side that depends on the current through the TEG and it contributes to the decrease of temperature between the TEG faces as compared to an open-circuit situation, when the current through the TEG is equal to zero. This is due to the Peltier effect. It also shows that there is a contribution from the internal Joule heating, but this contribution is smaller than the Petier effect [18]. If Q_H is maintained constant ΔT is maximum when no current is generated by the TEG. ΔT progressively decreases with an increase in electrical current. In order to maintain a constant temperature difference across the TEG device while the output current is increased, extra thermal energy must be transferred into the system to compensate for the Peltier effect contribution. This is not possible with limited heat sources.
There are many applications where the amount of heat is limited and therefore it is not possible to maintain a constant temperature across the TEG while the TEG current varies. Previous studies [20]–[26] have shown that under these conditions the maximum power delivered by the TEG is not produced when $R_{TEG} = R_{load}$. The optimum external load is related to the figure of merit ZT as shown in Eq.(3):

$$\frac{R_{load}}{R_{TEG}} = \sqrt{1 + Z\overline{T}} \tag{3}$$

whose parameters vary with the average temperature of the TEG device and therefore it is not possible to establish a fixed value for the optimum load when the temperature across the TEG varies.
Recent studies have shown that the MPP of TEGs operating under constant heat flux is found when $\beta > 0.5$. Montecucco et al. [26] supports this argument through the use of theoretical simulations confirmed by the work of Min [27] . These studies also show that the ratio β at which the MPP is achieved changes with the amount of heat flux through the TEG.
Maximum power point tracking (MPPT) systems use DC-DC converters to operate the TEG at the MPP. This is achieved by controlling the input current or voltage of the converter so that the TEG operates at the MPP.
Some of the most common MPPT techniques used, like P&O or IC, change the operating point of the TEG by monitoring (sampling) the output power of the device until the MPP is reached. The dynamic response of the system must be taken into consideration so that the MPPT algorithm measures the correct steady-state value of power, otherwise the power converter will not be able to track the correct MPP.
Traditional MPPT algorithms like P&O or IC operate using sampling times that are several orders of magnitude shorter than the thermal time constants of TEG systems. The thermal time constant of a TEG system is defined in this paper as the time required for the system to change 63.2% the total difference between the initial and final temperature across the TEG plates when a load step change is applied at its terminals. The thermal time constant depends on the thermal resistance and the thermal capacitance of the different elements in the system, such as heat exchangers, thermoelectric device and the interfaces between these elements. A practical MPPT development is sensitive to the size and thermal time response of the system in use, hence the MPPT response parameters might need to be tuned to the particular system where it is used to achieve optimal performance.

Changing the operating point of a TEG at fast frequencies (compared to the thermal time constant of the system) will not allow for temperature changes across the TEG, which would be equivalent to operate at constant ΔT between consecutive samples. Without allowing the TEG system to reach steady-state conditions it is not possible to track the MPP under constant input heat flux.
In this paper the results of a study into the transient response of the TEG using power curves, obtained under conditions of constant heat flux and constant ΔT, are presented. The behaviour is then verified using experimental data. The effects of the dynamic response are shown using a boost (step-up) converter controlled by a microcontroller that implements a P&O algorithm.

2. Dynamic Response

This section presents an analysis of the dynamic response of a TEG operated under constant heat flux conditions. Nonetheless, the electrical characteristic curves for constant temperature difference are also fundamental to aid the behaviour of the TEG in a thermally dynamic environment.
Any change in the operation conditions of a TEG operating under constant heat flux will occur at constant temperature. This is because the temperature of the system will not change instantaneously when the operating condition is changed. This effect is only valid at the moment the load change is applied. The temperature across the TEG will then change until the system reaches a new steady-state condition. This change in temperature is due to the Peltier effect that changes the effective thermal resistance of the TEG. The new steady-state condition corresponds to the crossover point between the constant heat flux power curve and the constant temperature power curve obtained at the new temperature difference across the TEG. For this reason it is important to inspect both types of curves in order to understand the transient response of the TEG. These transitions will be explained with the aid of Figure 1 and Figure 2.
It has been shown in [26] that the maximum power point of a TEG operating under constant heat flux corresponds to a point where $\beta > 0.5$. Figure 1 shows the "Power and Voltage vs Current" curve of the TEG *GM250-241-10-12*[1] operating under a constant heat flux of 35W. The maximum power point and the voltage under these conditions are 0.57 W and 2.53 V respectively, and the open-circuit voltage is 4.97 V which corresponds to a $\beta = 0.626$.
The instantaneous open-circuit voltage versus temperature curve, in green, shows the instantaneous voltage across the TEG terminals when the load is removed. The instantaneous voltage versus temperature curve, orange, shows the instantaneous voltage across the TEG terminals when it operates under load. Both curves converge at zero output current.

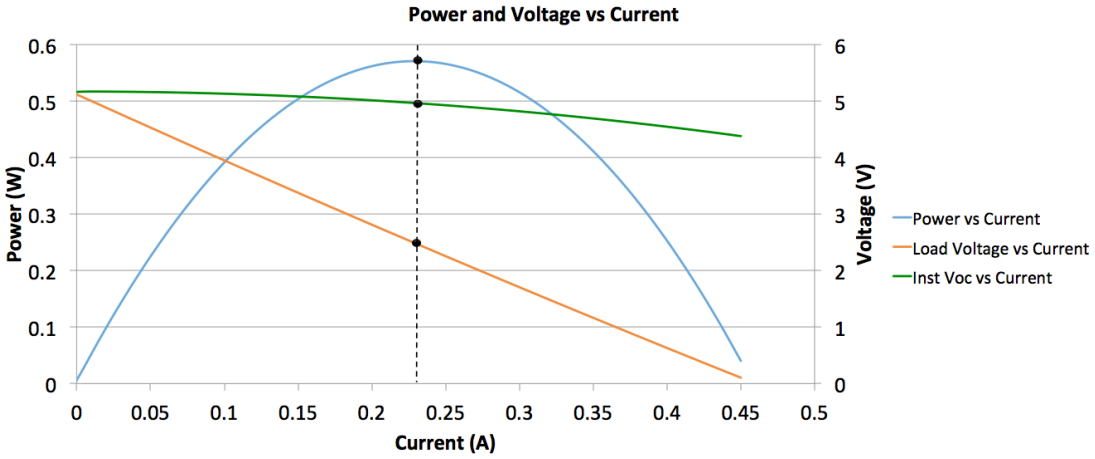

Figure 1 – Power (left y-axis) and Voltage (right y-axis) vs Current for a TEG operating under 35W constant heat flux

The curve shown in Figure 1 is obtained by measuring voltage and current, and multiplying these values to obtain power genearated by the TEG. The heater is driven using a power supply unit, load transients are produced using an electronic load, the hot and cold side temperatures are measured using a data acquisition unit and the output voltage and current of the TEG are measured using digital multimeters. More details of the equipment used is found in Table 2. Measurements have been taken every 50mA, a total of 10 points, and curve fitting has been used to produce the curve. The

[1] www.europeanthermodynamics.com

experimental points that make the curves shown in Figure 1 are obtained in steady-state conditions. Previous works have investigated the effect on temperatures due to short-circuit to open-circuit changes [28] and to fast load stepping for measurements under constant temperature difference [29].
The power-temperature curve of Figure 1 is not a symmetric parabola around the MPP. This can be seen from the fact that the MPP occurs at 0.225A, however, at 0.45A (double the value of I_{MPP}) the power generated by the TEG has not reached 0W; in other words, 0.45A does not correspond to the short-circuit current. The short circuit current is higher than 0.45A.
The voltage vs current line is not straight as it occurs under consant temperature difference (where its slope relates to the internal resistance of the TEG [30]). This behaviour is also reported by Min [27], who provides useful mathematical relations between parameters obtained under constant heat flux and those for constant temperature difference. Min also reports in his work the main differences between TEGs operating under constant heat flux and under constant temperature difference, which are the basis for finding the maximum power point in TEGs under those operating conditions. The relationships found in Min's work are: *i)* The matched load resistance for a TEG operating under constant heat flux is different from that when operating under constant ΔT, *ii)* For constant heat flux the matched resistance that maximises power output also maximises conversion efficiency, which is not the case for constant ΔT; *iii)* thermoelectric properties (α, ρ, λ and Z) change during I-V measurements and, therefore, during measurements of the TEG's power curvers. These relationships evidence the dependancy of the main thermoelectric parameters with temperature, and therefore the relationship of the maximum power point of the TEG with output current (due to the parasitic Peltier effect).
In order to understand the transient response of a TEG we must also plot the power curves for constant ΔT.

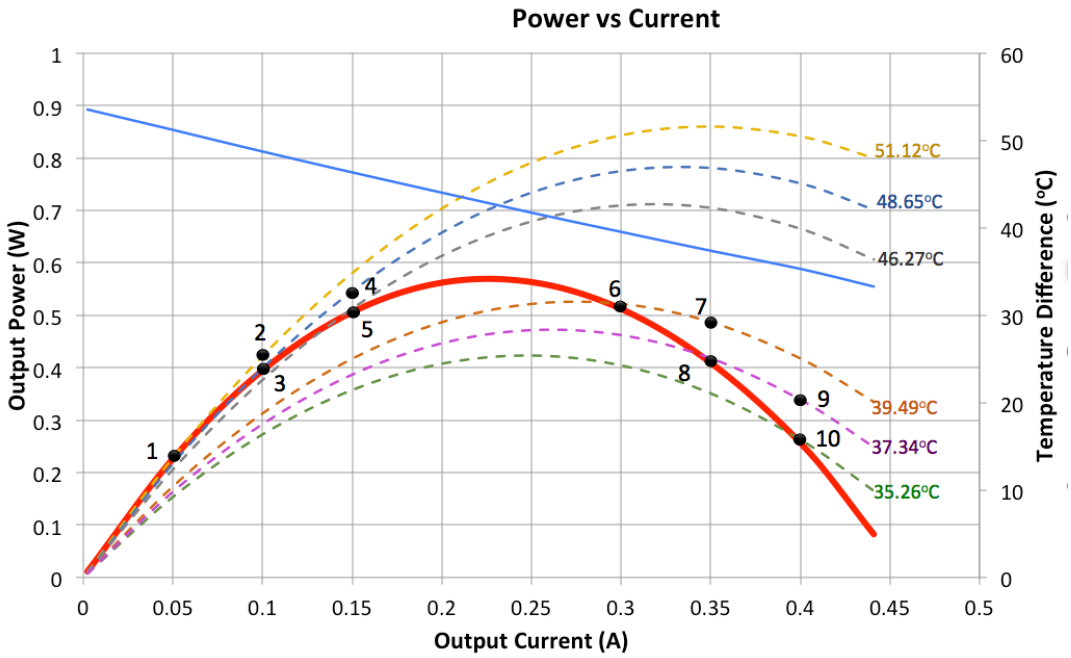

Figure 2 - Power curves for constant heat flux (35W, solid red line) and constant ΔT (dashed lines) with increasing load changes

Figure 2 shows the same power curve of Figure 1 and also the power curves for several constant temperatures under steady-state conditions. The solid red line shows the curve for constant heat flux and the dashed lines represent power curves for constant ΔT at different values of temperature difference, which are shown in the graph next to each curve. The solid blue line represents the steady-state temperature difference across the TEG. The solid black points marked in the curves correspond to different electrical points when the output load increases and are summarized in Table 1.

Point	Current (mA)	Power (mW)	ΔT (ºC)
1	50	237	51.12
2	100	430	51.12
3	100	400	48.65
4	150	541	48.65

5	150	509	46.27
6	300	510	39.49
7	350	472	39.49
8	350	406	37.34
9	400	321	37.34
10	400	253	35.26

Table 1 - Points marked in Figure 2 with increasing load changes TEG

The constant temperature curves have been obtained by using the equations of the TEG using Eq.(4) and Eq.(5) with the values for R_{INT} and V_{OC} obtained experimentally as described in [14] and presented in Eq.(6) and Eq.(7), respectively.

$$V_{OUT} = V_{OC} - (R_{INT} - I_{OUT}) \tag{4}$$

$$P_{OUT} = V_{OUT} \cdot I_{OUT} \tag{5}$$

$$R_{INT} = -0.00002 \cdot \Delta T^2 + 0.0231 \cdot \Delta T + 5.9357 \tag{6}$$

$$V_{OC} = -0.00003 \cdot \Delta T^2 + 0.098 \cdot \Delta T \tag{7}$$

If the TEG reaches steady-state at point 1, with 51.12°C across it, and a sudden load step from 50mA to 100mA is applied, the temperature difference across the TEG will not change immediately at the time the load step is applied. This is because the thermal capacitances of the system prevent the temperature from changing instantaneously. Hence the TEG continues to operate under the constant ΔT curve corresponding to 51.12°C, and the output power changes from 237mW (point 1) to 430mW (point 2). The output power then decreases exponentially, following the reduction in temperature gradient dictated by the thermal time constant of the system, from 430mW to a steady-state power of 400mW (point 3). Once steady-state is reached, the temperature difference across the TEG has decreased from 51.12 °C to 48.65 °C. When a second load step is applied from 100mA to 150mA the output power changes immediately from 400mW (point 3) to 541mW (point 4). Progressively the TEG reaches steady-state conditions delivering 509mW with a ΔT of 46.27 °C (point 5). This behaviour will be observed with increasing load changes up to the MPP.

When increasing load changes are applied past the MPP, *i.e.* to the right of the MPP as shown in Figure 2, the behaviour is similar to the previous situation, following the transitions across constant ΔT curves, with decreasing output power and temperature. If the TEG was operated under steady-state condition at point 6, with ΔT=39.49 °C, and a step load is applied from 300mA to 350mA, the power decreases immediately from 510mW to 472mW (point 7). Once the system reaches steady-state (point 8) the power decreases further to 406mW and the temperature decreases to 37.34 °C. When another load step is applied from 350mA to 400mW the output power decreases immediately from 406mW to 321mW (point 9) and at steady-state it becomes 253mW with ΔT=35.26 °C.

Figure 3 shows the different transitions when the load current is stepped down.

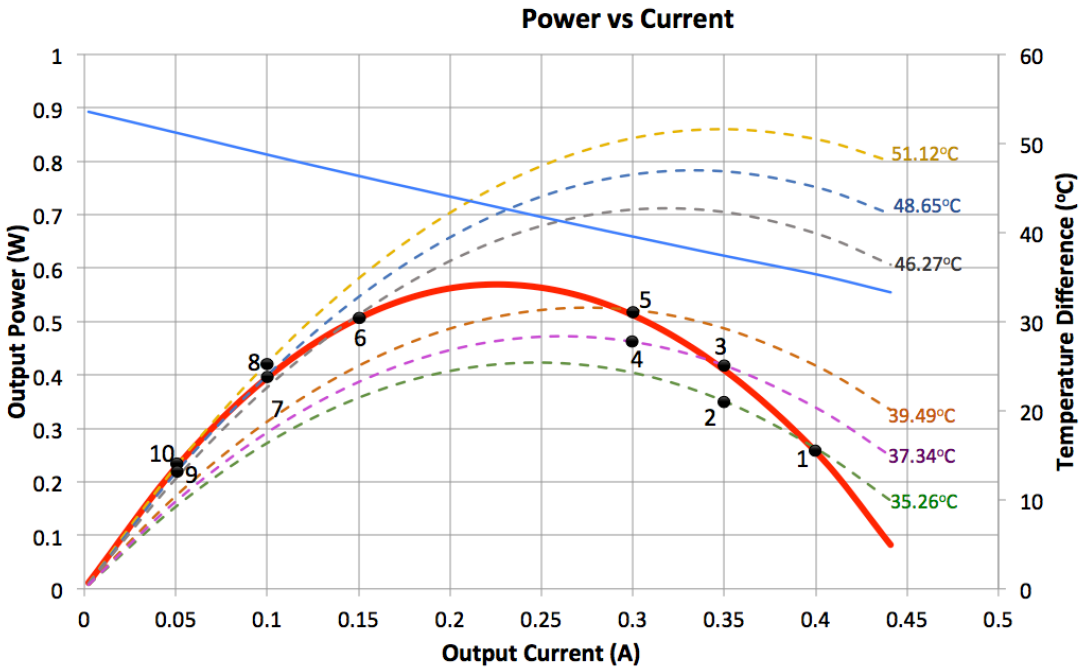

Figure 3 - Power curves for constant heat flux and constant ΔT with decreasing load changes

The same principles apply when moving from higher to lower load currents. The temperature difference across the TEG does not change immediately due to the thermal capacitance of the system and there will be transitions between constant ΔT and constant heat flux power curves. The points marked in Figure 3 are numbered in the order the transitions occur. Transitions across the same constant ΔT curve occur immediately whereas the transitions between a constant ΔT curve and the constant heat flux curve correspond to exponentially increasing or decaying transitions dictated by the thermal resistances and capacitances of the system. The difference between the thermal and electrical time constants is several orders of magnitude: depending on the electrical reactances in the circuit, settling time is usually measured in the order of nanoseconds where as for the thermal response the settling time is many minutes [31]. This difference in time constants poses a particular challenge to the development of an MPPT algorithm that is able to simulateously accommodate the thermal and electrical responses to determine the true MPP.

3. TEG Test Fixture

The test fixture used to obtain the transient response of the TEG to step load changes is similar to the one described in [30] and it is represented in a schematic diagram in Figure 4 (left). A picture of the test rig is also shown in Figure 4 (right).

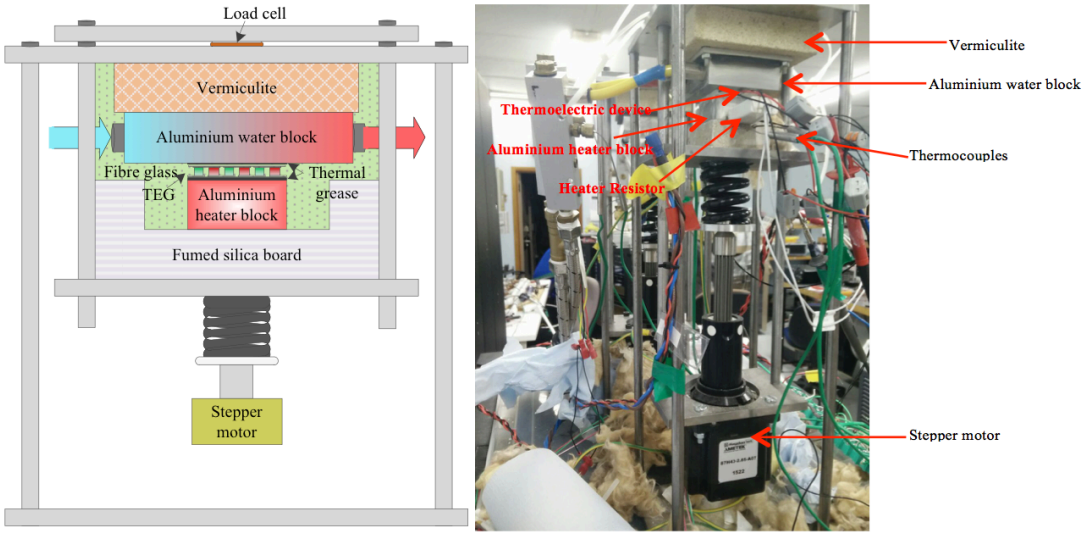

Figure 4 - Test fixture used to characterize the response of the TEG, schematic diagram (left) and test rig (right)

The system uses an aluminium water-cooled heatsink block at the top that is used as the cold side temperature reference of the TEG. The temperature of the water is controlled and kept constant using a chiller that keeps the heatsink temperature at approximately 25°C. Heat is provided to the system by a resistive electrical heater placed inside an aluminium heater block placed underneath the TEG, with same surface area of contact. The heater is controlled by a power supply to meet the desired test conditions. A fumed silica board and fibre glass are used around the TEG assembly to reduce radiation and convection losses to ambient. The clamping force of the TEG between the water and heater blocks is controlled with a stepper motor and can be adjusted to meet the desired clamping force. The load cell is the sensor that measures the clamp force across the thermoelectric device. Temperature and electrical measurements are performed by a datalogger and all instruments are controlled by a VEE pro®[2] PC interface. A more accurate description can be found in [30] with the main difference being that the stepper motor is placed on the top of the test rig.

The thermal system is not perfectly insulated and part of the heat generated by the heater block is lost to the surrounding environment. Extra heat is injected into the system to compensate for these losses and the amount of heat required can be calculated using Eq.(8) [32].

$$Q_{losses} = 3 \cdot 10^{-5} \cdot {T_H}^2 + 0.0357 \cdot T_H \tag{8}$$

Eq. (8) has been obtained experimentally by using a vermiculite block instead of a TEG to minimize the amount of heat going to the cold side. By keeping the cold side temperature close to ambient, 25°C, it can then be assumed that most of the heat is being lost to the environment and therefore the input power can be approximated to the heat losses. The method is explained in [32]. This equation is valid for temperatures in the hot side above 40°C, which are the temperatures reached on the hot side during the experiment and represent an approximation of the heat losses. The equation shows a loss of 3.176W when the hot side temperature is equal to 80°C, which is the maximum hot side temperature reached in our experiments. With an input power of 35W, the losses represent 9.07% of the total input power.

The same *GM250-241-10-12* device and thermal conditions discussed in Section 1 have been used to obtain the experimental results presented in this section. In the next experiments the load current obtained from the TEG is adjusted in 50 mA increments or decrements and the voltage, current, hot side and cold side temperatures are monitored every 9 seconds. It is important to select a current step size that evidences the shape of the TEG's transient response. Current steps of 50 mA have been selected experimentally to make the transient response at 35W stand out, as it is seen in Figure 5. The sampling time has to be small enough so that a sufficient amount of data points can be obtained to be able to plot the transient response with accuracy. On the other hand, too many data points will provide large files that could lead to a cumbersome acquisition program. For a "slow" thermal transient response, a sampling time of 9 seconds is enough to provide an accurate plot of the transient response.

[2] www.keysight.com

4. Transient Response: Experimental Results

Two different characterisations have been performed on the *GM250-241-10-12* device using the test rig presented in the previous section.
The equipment used during the experiment is the following:

Equipment	Model	Function
Power Supply Unit	Agilent N5750	Drive the heater placed in the heater block
Electronic Load	Agilent N3300A	Provide load changes on the TEG
Data Acquisition Unit	Agilent 34972A	Acquisition of the hot and cold side temperatures
Digital Multimeter	Agilent 34410A	Measure the output current of the TEG
Digital Multimeter	Agilent 34405A	Measure the output voltage of the TEG

Table 2 - List of the test equipment used for the transient response test

Figure 5 plots the variation of load voltage and power versus time resulting from increasing the electrical current from open-circuit to 450 mA, in steps of 50 mA.

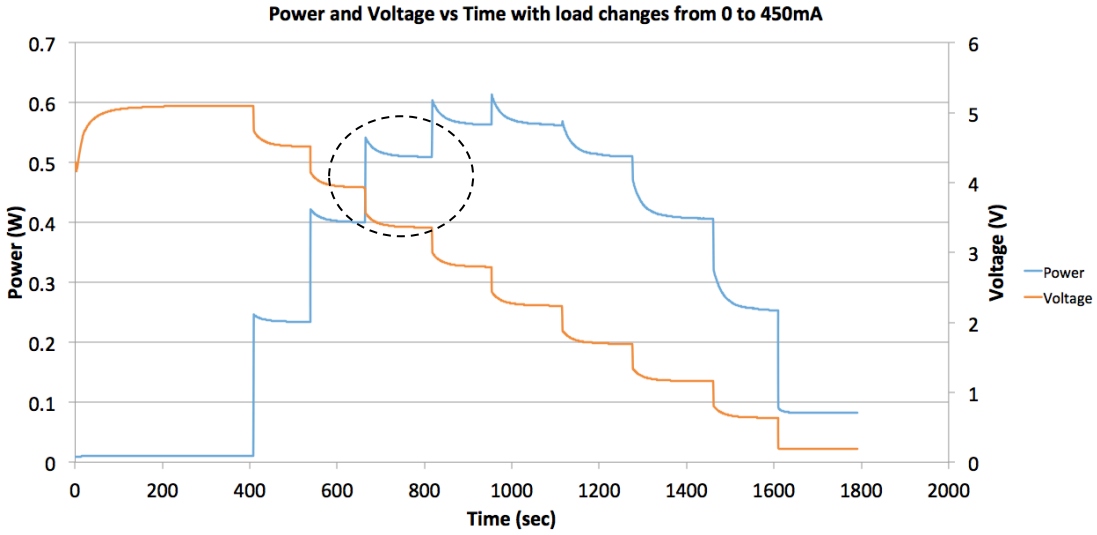

Figure 5 – Power (left y-axis) and voltage (right y-axis) curves showing the transient response of the TEG versus time (x axis) when the TEG current is progressively increased from open-circuit to 450mA.

Figure 5 provides information about the transition between constant ΔT curves. The dynamic response shows an exponential decay to steady state. If the steady-state points of Figure 5 were plotted against the output current then the curve of Figure 1 would be obtained. Figure 6 shows an enlargement of the area encircled in Figure 5, and provides an insight into the transitions described in Figure 2. On the left side of Figure 6 the TEG is operating in steady-state conditions with a load current of 100mA and an output power of 400mW. When the load changes from 100mA to 150mA the output power increases instantaneously from 400mW to 541mW and then it decreases exponentially down to 509mW. The transient response corresponds to a first order system the time constant of which is dictated by the thermal resistances and thermal capacitances of the TEG system. It is out of the scope of this article to calculate the thermal resistance and capacitance that dictates the time constant of the system. References about articles and technical notes that calculate these parameters are provided [42], [43]. These transitions correspond to points 3, 4 and 5 of Table 1. The output voltage also changes following the same principles. In steady state the output voltage is 3.92V and it then changes instantly to 3.57V. This corresponds to an instantaneous change of voltage across the same ΔT=48.65 ^{o}C constant temperature curve, then reaching steady-state at 3.35V.

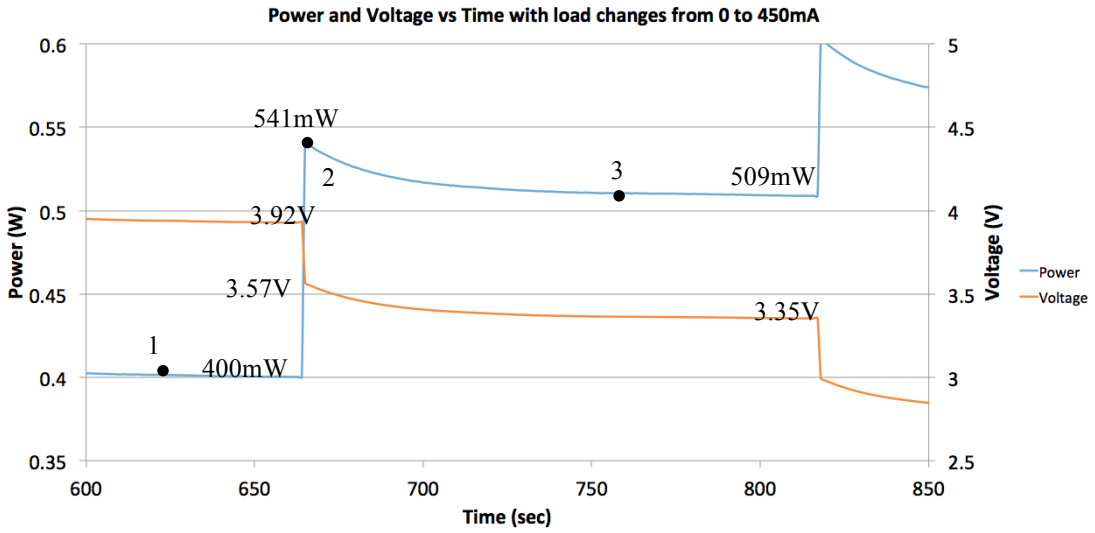

Figure 6 – Enlarged view of the encircled area of Figure 5

When the load current is progressively reduced from short-circuit current to zero (open-circuit), the temperature across the TEG increases therefore the transitions occur towards higher ΔT curves. The transient response showing the output power and voltage in a TEG under these load steps is shown in Figure 7.

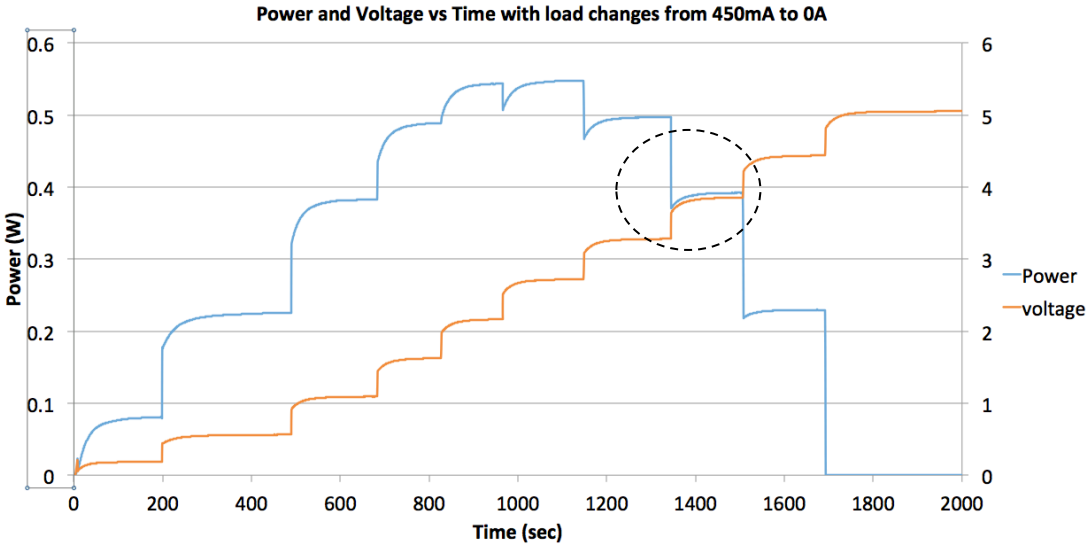

Figure 7 - Power (left y-axis) and voltage (right y-axis) curves showing the transient response of the TEG versus time (x axis) when the TEG current is progressively decreased from short-circuit to open-circuit.

The graphs show both the instantaneous transitions across constant ΔT curves and the exponential transitions towards steady-state. Figure 8 provides an enlarged view of the encircled area in Figure 7 where the transitions between points 6, 7 and 8 in Figure 3 are labeled with their corresponding values.

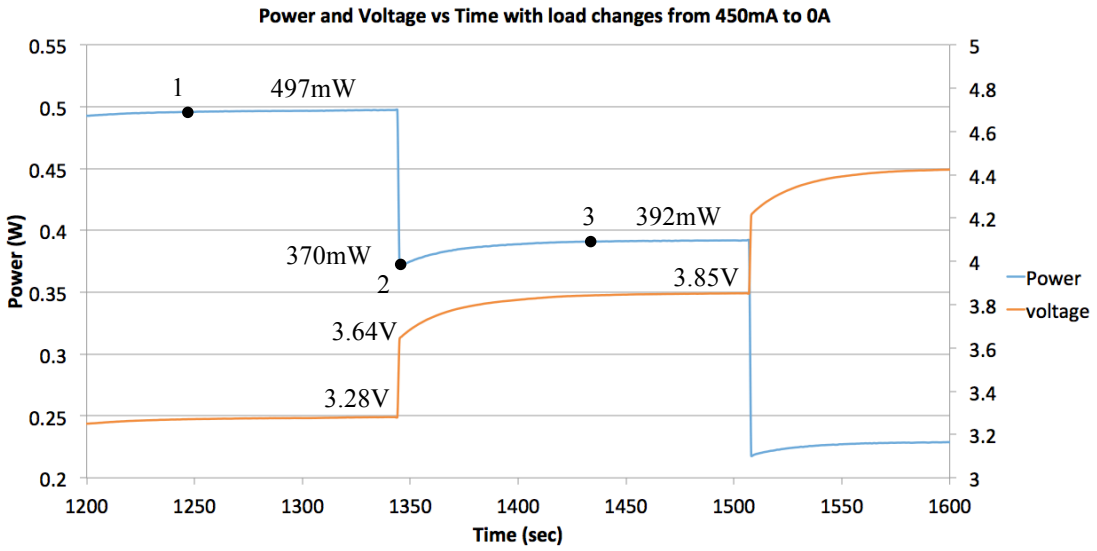

Figure 8 – Enlarged view of the encircled area of Figure 7

5. Maximum Power Point Tracking Errors

There are different ways to implement MPPT for thermoelectric devices [33], [34], and most of these methods are inherited from photovoltaic (PV) systems. The most common methods are fractional open-circuit (FOC) voltage [35], Perturb and Observe (P&O) [36], [37] and Incremental Conductance (IC) [38].

The FOC method regulates the TEG voltage at a fixed percentage of the open-circuit voltage [39], [40]. When used in constant ΔT applications the TEG voltage is regulated at half of the instantaneous open-circuit voltage, *i.e.* the voltage that the TEG would generate in open-circuit at the actual temperature difference. This operating point is chosen because for any constant ΔT curve, the maximum power point corresponds to half of the open-circuit voltage.

P&O and IC are generally known as "hill climbing" algorithms: the electrical operating point of the TEG is continuously perturbed and the instantaneous power delivered is compared to the power measured in the previous iteration. The algorithm effectively climbs along the power curve towards its peak power point (MPP).

In a practical dynamic application the temperature profile is influenced both by the input thermal power to the TEG hot (or from the cold) side and by the electrical current provided by the TEG to the load. Consider now that the TEG is driven by a constant heat source and it is left in open-circuit until thermal equilibrium is reached at ΔT = 51.12°C. With the aid of Figure 9, to this initial temperature state is associated a constant ΔT curve (yellow, dotted). Operating the TEG at half of the open-circuit voltage (FOC at 50%) corresponds to working at the MPP of that particular constant ΔT curve (point 1). As explained in [26] and following Eq. (2), the temperature across the TEG starts to decrease because the electrical current generated by the TEG gives rise to the Peltier effect, undersired in power generation. After a thermal transient whose length depends on the thermal fluxes and heat capacities of the system, the TEG will be subject to a lower ΔT of 46.27°C, to which a new constant ΔT curve is related (grey, dotted). The electrical load is changed to the new MPP of this "new" curve (point 2 in Figure 9). When the temperature difference decreases to 42.4°C, and the load is changed to the new MPP of the power curve for that temperature, the operating point is moved to point 3 of Figure 9.

The operation here described assumes that the electrical operating point changes discontinuously at time intervals for sufficiently long for temperatures to settle even after large temperature changes.

The steps described in the previous paragraph are repeated until the TEG is operated at a temperature difference for which the MPP of the constant ΔT curve associated to it lies also on the power curve for constant heat flux (point 4 in Figure 9). It is clear from Figure 9 that the point reached in the constant heat flux curve is not the real MPP. Point 4 corresponds to the MPP at ΔT=39.9°C, and it is also the final steady-state point because this point also corresponds to a point in the constant heat flux curve. However, the MPP of the curve for constant heat flux is point 5 of Figure 9. This point is obtained generating less current at higher voltage compared to point 4. Although point 5 is not the MPP of the

constant ΔT curve (in fact, it would be point 3) it lies also on the peak of the curve for constant heat flux.

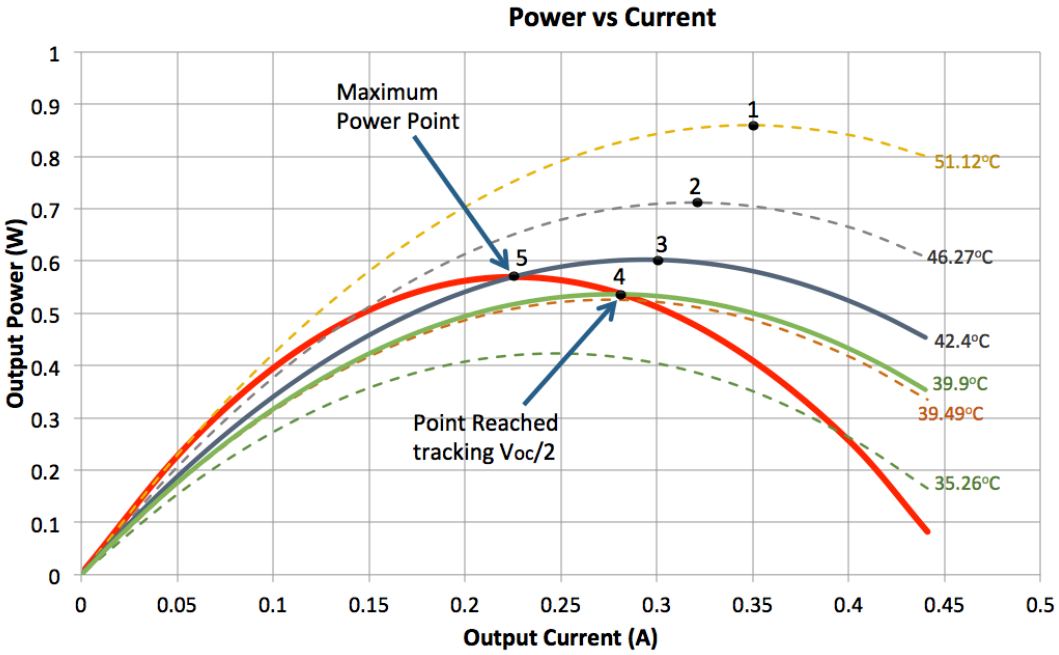

Figure 9 - Maximum power point and MPPT errors

Figure 9 shows that the power curve in constant heat flux (bold red) has a parabolic shape similar to that of a constant ΔT curve. As a consequence, it seems straightforward that a ¨hill climbing¨ MPPT algorithm, e.g., P&O, would find the optimum operating point for TEGs also under constant heat flux conditions. However, common P&O algorithms developed for solar PV systems have sampling frequencies in the order of few tens of Hertz [41]. As it can be seen in Figure 5 and Figure 7 the thermal time constant of the system used is approximately one minute. This in turn means that a "fast" P&O algorithm (considering as "fast" the sampling rates of a conventional P&O for PV systems) would not be able to account for the thermal transients due to variations in the output current, because they have a time constant significantly greater than the sampling time of the algorithm. Hence the P&O algorithm would quickly settle on the MPP of the actual constant ΔT curve. For this reason, it would operate the TEG exactly as described above in this section, *i.e.* eventually settling at point 4 of Figure 9. Significantly reducing the sampling rate of the P&O algorithm to allow for thermal transients to evolve after each load perturbation would allow for effective tracking of the MPP for constant heat flux. As shown in Figure 9 the sampling time should allow for at least 4 thermal time constants before taking measurements, otherwise it could be deceived. As the thermal time constant is related to every particular TEG system, it is not straightforward to decide the optimal sampling time a priori. However, reducing the sampling time severely affects the transient response to external events, e.g., thermal energy and temperature variations. A possible solution to this problem is to sense and establish when the system has reached thermal steady state following a known load perturbation. Moreover, in a practical system the input thermal energy varies depending on the heat source and a reliable MPPT algorithm is required to account for "unknown" thermal variations due to external causes.

6. TEG Operated Under Constant Heat Flux and the Maximum Power Transfer Theorem

It is well known that under constant temperature conditions, the MPP is reached when the value of the output load is equal to the value of the internal resistance of the TEG, as indicated by the maximum power transfer theorem. The load voltage under these conditions is equal to half of the open-circuit voltage of the TEG and β=0.5.

Under constant heat flux the maximum power point is produced when β>0.5, which corresponds to a load voltage that is higher than half of the open-circuit voltage of the TEG. This point is equivalent to point 5 in Figure 9, with ΔT=42.4°C. At this point the internal resistance of the TEG is not equal to the load resistance, however the TEG is not operated at the MPP of the ΔT=42.4°C curve; that is, point 3.

At point 3, the internal resistance of the TEG is equal to the load resistance and the conditions dictated by the maximum power transfer theorem are met.
It is important to note that, if the TEG operates at β=0.5, the output power would decrease due to the limited heat provided by the source (constant heat flux) and the power delivered by the TEG would decrease to point 4; where β=0.5 but the power delivered is lower than that in point 3.

7. Experimental Results

A boost (step-up) dc-dc converter has been designed to verify the operation of the TEG under constant input heat flux conditions; the schematic diagram of the power converter is shown in Figure 10, where the TEG has been modeled as a voltage source with a series resistor that represents the internal resistance of the TEG. The current (I) is measured using a current sensor that measures the voltage across a shunt resistor in series with the output of the TEG. The sensor produces a voltage (V) across R_L proportional to the TEG's output current. Voltage is measured using a potential divider connected across the output terminals of the TEG. The variables V and I are scaled down for compatibility with the voltage reference of the analogue-to-digital converter of the microcontroller. A gate driver is used to provide the current required for a fast switching operation of the power MOSFET. The boost converter is used to charge a Li-ion battery, which can be considered as a constant voltage at the output of the converter.

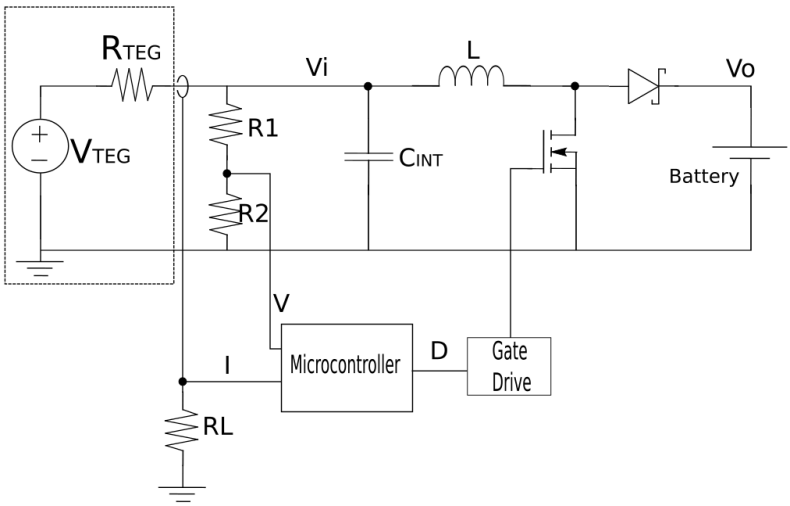

Figure 10 - Circuit diagram of the Boost power converter

The control of the power converter is performed with a microcontroller that implements P&O and the control scheme is shown in Figure 11. This type of control can be implemented in embedded systems. The P&O algorithm implemented finds the MPP by comparing the power generated by the TEG against the value of power measured in the previous iteration. The time between power samples is around 4 times the time constant of the TEG system, which allows enough time for the microcontroller to capture the steady-state value of power. Because the converter controls the power generated by a single thermoelectric device, the algorithm does not implement any mechanism to be able to reject local maxima.
The algorithm starts-up setting the initial operating point of the TEG in open-circuit and performs the operations described in Figure 11. Note that the speed of the algorithm could be improved by setting the initial operating point to half of the open-circuit voltage.
It is important to decide on the size of the duty-cycle change in order to improve the speed of the algorithm. As it can be seen in Figure 1, the power delivered by the TEG changes to a small extent in the vicinity of the MPP. The algorithm applies small changes in duty-cycle, 0.3125%, in the vicinity of the MPP and bigger changes, 1.25%, otherwise. 0.3125% is the minimum change in duty-cycle the microcontroller used can provide. Increasing the minimum duty-cycle by a factor of four; that is, 1.25%, has been experimentally found to be a good compromise between MPP tracking speed versus magnitude of oscillations around the MPP.

The direction of the perturbation is dictated by comparing the value of power generated by the TEG against previous measurements. The latest measured power P is saved as it is used in the next program iteration as P_O.
This work has not analysed the effect of measurement noise and explored ways for the algorithm to recover from such instances and erroneous/unexpected behaviour.

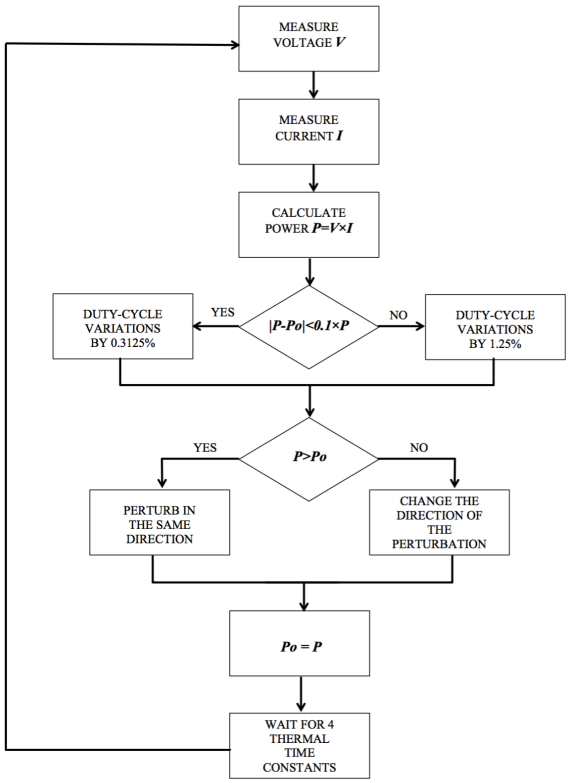

Figure 11 - Flowchart of the P&O MPPT algorithm controlling the Boost converter

The power converter described above in this section is interfaced to the TEG system described in Section 1 and 2, operated under constant heat flux. Figure 12 shows a graph of the power and voltage generated by the TEG during 700 seconds of operation with a constant heat flux of 35W. The power generated by the TEG differs by less than 30mW from the MPP shown in Figure 1, which corresponds to a 5.2% difference with respect to the peak power in Figure 1. Nonetheless, the voltage set point is correct, therefore this small difference in power production is attributed to measurement errors in the power converter board (especially in current measurements) as well as in small differences in thermal conditions between the two experiments. The most interesting characteristic of the traces in Figure 12 are the shape of the power and voltage transitions which correspond to those observed in Figure 5 and Figure 7.

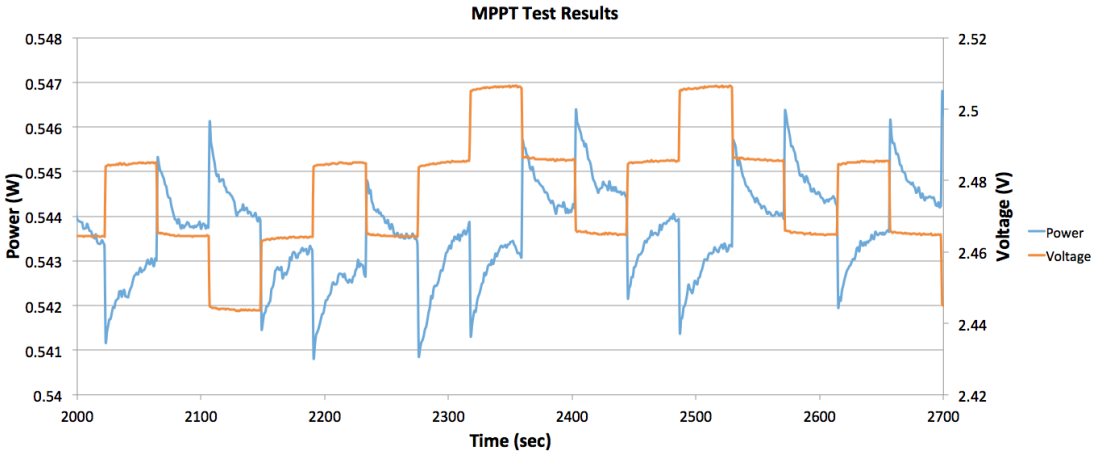

Figure 12 - MPPT test results

It can also be observed that there are only two transitions in one direction before the P&O algorithm changes the direction of the perturbation, indicating that the power delivered by the TEG oscillates around a maximum point that corresponds to the MPP. This is also the desirable behaviour, as minimizing the oscillations around the MPP helps to maximize the power generation, as the operating point does not move far from the MPP; as well as minimizes the amount of voltage and current ripple at the terminals of the TEG.

8. Conclusions

The transient response of the TEG is the typical of a first order system, with transitions along constant ΔT curves. Experimental results of the transient response are shown when electrical load step changes are applied to a TEG that operates under constant heat flux. The time constant of the TEG system is an important factor to take into consideration when designing MPPT algorithms, as the shape of the transient response could lead to tracking errors, as explained in Section 5. The slowly changing thermal system is to be expected and any algorithm applied to the control task must be matched to the physical parameters. The option explored in this article is, indeed, to wait for a relatively long time before samples are taken and processed, and the system is perturbed to the next operating point.

These results show that MPPT algorithms used for PV systems that use fast sampling rates, that are orders of magnitude greater than the typical thermal time constant of a TEG system, are not adequate for thermoelectric systems.

An experimental application using a boost dc-dc converter controlled by a P&O algorithm further demonstrates the performance of a TEG operated under constant heat flux conditions. Experimental results show the characteristics of the transient response when the operating point of the TEG is perturbed. The MPPT algorithm is demonstrated to operate the TEG in close proximity of its MPP for constant heat flux conditions, proving that allowing for the transient response to subside between two consecutive samples helps minimizing oscillations and tracking errors.

In a real TEG system the thermal time constant might vary with external temperature conditions or mechanical variations in the TEG system that could affect the thermal capacitances and resistances of the system.

A fixed sampling time might provide wrong results if the thermal time constant of the system increases or might lead to unnecessary waiting time if the thermal time constant decreases. In other instances, *e.g.*, vehicle exhaust systems, the available heat flux is unlikely to be constant [11]. In order to overcome this issue, the algorithm must monitor the output power constantly in order to assess when it has reached its steady-state value. By doing so, the performance of the algorithm will not be influenced by changes in the thermal time constant or heat flux through the system as it ensures that all the power samples computed to decide on the next perturbation correspond to points of the constant flux power characteristic curve. Moreover, the MPPT system must identify external changes in the operating conditions to ensure fast tracking performance during transients. These features represent the topic of future work because they are fundamental to the design of an effective MPPT algorithm capable of strong performance in practical TEG systems at steady state and during transients.

Other MPPT techniques to be explored are based on adaptive MPPT algorithms where the changes in duty cycle are proportional to the rate of change of power with respect to voltage (dP/dV). These techniques are explained in [44] and [45] and help reducing the step size in the proximity of the MPP thus reducing the oscillations during steady-state. Extremum-Seeking Control (ESC) techniques, [46] and [47], are employed when the power curve of the device to be controlled is non-linear and unknown and can also be employed for TEG systems whose characteristics are subject to change with time.

Acknowledgements

The authors would like to thank the Engineering and Physical Sciences Research Council (EPSRC), the Energy Technology Partnership (ETP) and Clyde Space Ltd. for the funding provided for this project.

References

[1] W. He, G. Zhang, X. Zhang, J. Ji, G. Li, and X. Zhao, “Recent development and application of thermoelectric generator and cooler,” *Appl. Energy*, vol. 143, pp. 1–25, 2015.

[2] D. G. Ebling, A. Krumm, B. Pfeiffelmann, J. Gottschald, J. Bruchmann, A. C. Benim, M. Adam, R. Labs, R. R. Herbertz, and A. Stunz, "Development of a System for Thermoelectric Heat Recovery from Stationary Industrial Processes," *J. Electron. Mater.*, 2016.
[3] P. Aranguren, D. Astrain, A. Rodríguez, and A. Martínez, "Experimental investigation of the applicability of a thermoelectric generator to recover waste heat from a combustion chamber," *Appl. Energy*, vol. 152, pp. 121–130, 2015.
[4] S. M. O. Shaughnessy, M. J. Deasy, J. V Doyle, and A. J. Robinson, "Performance analysis of a prototype small scale electricity-producing biomass cooking stove," *Appl. Energy*, vol. 156, pp. 566–576, 2015.
[5] D. Champier, J. P. Bédécarrats, T. Kousksou, M. Rivaletto, F. Strub, and P. Pignolet, "Study of a TE (thermoelectric) generator incorporated in a multifunction wood stove," *Energy*, vol. 36, no. 3, pp. 1518–1526, Mar. 2011.
[6] A. Montecucco, J. Siviter, and A. R. Knox, "Combined heat and power system for stoves with thermoelectric generators," *Appl. Energy*, vol. 185, pp. 1336–1342, 2017.
[7] G. Min and D. Rowe, "'Symbiotic' application of thermoelectric conversion for fluid preheating/power generation," *Energy Convers. Manag.*, vol. 43, no. 2, pp. 221–228, Jan. 2002.
[8] M. P. Codecasa, C. Fanciulli, R. Gaddi, F. Gomez-Paz, and F. Passaretti, "Design and Development of a TEG Cogenerator Device Integrated into a Self-Standing Natural Combustion Gas Stove," *J. Electron. Mater.*, Aug. 2014.
[9] Y. Wang, C. Dai, and S. Wang, "Theoretical analysis of a thermoelectric generator using exhaust gas of vehicles as heat source," *Appl. Energy*, vol. 112, pp. 1171–1180, Dec. 2013.
[10] S. Risse and H. Zellbeck, "Close-Coupled Exhaust Gas Energy Recovery in a Gasoline Engine," *Res. Therm. Manag.*, vol. 74, pp. 54–61, 2013.
[11] S. Kumar, S. D. Heister, X. Xu, J. R. Salvador, and G. P. Meisner, "Thermoelectric Generators for Automotive Waste Heat Recovery Systems Part I: Numerical Modeling and Baseline Model Analysis," *J. Electron. Mater.*, vol. 42, no. 4, pp. 665–674, Feb. 2013.
[12] L. Merotto, C. Fanciulli, R. Dondè, and S. De Iuliis, "Study of a thermoelectric generator based on a catalytic premixed meso-scale combustor," *Appl. Energy*, vol. 162, pp. 346–353, 2016.
[13] F. P. Brito, J. Martins, E. Hançer, N. Antunes, and L. M. Gonçalves, "Thermoelectric Exhaust Heat Recovery with Heat Pipe-Based Thermal Control," *J. Electron. Mater.*, 2015.
[14] A. Montecucco, J. Siviter, and A. R. Knox, "The effect of temperature mismatch on thermoelectric generators electrically connected in series and parallel," *Appl. Energy*, vol. 123, pp. 47–54, 2014.
[15] R. Decher, Direct Energy Conversion: fundamentals of electric power production. Oxford University Press, 1997.
[16] D. M. Rowe, *Thermoelectrics handbook: macro to nano*, vol. 80, no. 10. CRC Press, 2005.
[17] S. Lineykin and S. Ben-Yaakov, "Modeling and Analysis of Thermoelectric Modules," *IEEE Trans. Ind. Appl.*, vol. 43, no. 2, pp. 505–512, 2007.
[18] A. Montecucco, J. R. Buckle, and A. R. Knox, "Solution to the 1-D unsteady heat conduction equation with internal Joule heat generation for thermoelectric devices," *Appl. Therm. Eng.*, vol. 35, pp. 177–184, Mar. 2012.
[19] C.-Y. Du and C.-D. Wen, "Experimental investigation and numerical analysis for one-stage thermoelectric cooler considering Thomson effect," *Int. J. Heat Mass Transf.*, vol. 54, no. 23–24, pp. 4875–4884, Nov. 2011.
[20] G. Min and N. M. Yatim, "Variable thermal resistor based on self-powered Peltier effect," *J. Phys. D. Appl. Phys.*, vol. 41, no. 22, p. 222001, Nov. 2008.
[21] P. M. Mayer and R. J. Ram, "Optimization of Heat Sink–Limited Thermoelectric Generators," *Nanoscale Microscale Thermophys. Eng.*, vol. 10, no. 2, pp. 143–155, Jul. 2006.
[22] D. Nemir and J. Beck, "On the Significance of the Thermoelectric Figure of Merit Z," *J. Electron. Mater.*, vol. 39, no. 9, pp. 1897–1901, Jan. 2010.
[23] K. Yazawa and A. Shakouri, "Cost-efficiency trade-off and the design of thermoelectric power generators.," *Environ. Sci. Technol.*, vol. 45, no. 17, pp. 7548–53, Sep. 2011.
[24] Y. Apertet, H. Ouerdane, O. Glavatskaya, C. Goupil, and P. Lecoeur, "Optimal working conditions for thermoelectric generators with realistic thermal coupling," *EPL (Europhysics Lett.*, vol. 97, no. 2, p. 28001, Jan. 2012.
[25] R. McCarty, "Thermoelectric Power Generator Design for Maximum Power: It's All About ZT," *J. Electron. Mater.*, vol. 42, no. 7, pp. 1504–1508, Oct. 2012.
[26] A. Montecucco, J. Siviter, and A. R. Knox, "Constant Heat Characterisation of Thermoelectric Generators and Optimisation of Pellets Packing Factor," *Appl. Energy*, vol. 149, pp. 248–258, 2015.

[27] G. Min, “Principle of determining thermoelectric properties based on I – V curves,” *Meas. Sci. Technol.*, vol. 25, no. 85009, 2014.
[28] J. Gao and M. Chen, “Beat the Deviations in Estimating Maximum Power of Thermoelectric Modules,” *IEEE Trans. Instrum. Meas.*, vol. 62, no. 10, pp. 2725–2729, Oct. 2013.
[29] S. B. Mahajan, R. D. Pierce, and R. J. Stevens, “Characterizing high temperature thermoelectric modules,” in *ASME International Mechanical Engineering Congress and Exposition (IMECE2013)*, 2013, pp. 1–10.
[30] A. Montecucco, J. Buckle, J. Siviter, and A. R. Knox, “A New Test Rig for Accurate Nonparametric Measurement and Characterization of Thermoelectric Generators,” *J. Electron. Mater.*, vol. 42, no. 7, pp. 1966–1973, Mar. 2013.
[31] L. Chen, D. Cao, H. Yi, and F. Z. Peng, “Modeling and power conditioning for thermoelectric generation,” in *IEEE Power Electronics Specialists Conference*, 2008, pp. 1098–1103.
[32] Elena Anamaria Man, "Design considerations for thermoelectric power generation". PhD thesis, Aalborg University, July 2016.
[33] O. Maganga, N. Phillip, K. J. Burnham, A. Montecucco, J. Siviter, A. Knox, and K. Simpson, “Hardware Implementation of Maximum Power Point Tracking for Thermoelectric Generators,” *J. Electron. Mater.*, Feb. 2014.
[34] S. Twaha, J. Zhu, Y. Yan, and B. Li, “A comprehensive review of thermoelectric technology : Materials , applications , modelling and performance improvement,” *Renew. Sustain. Energy Rev.*, vol. 65, pp. 698–726, 2016.
[35] A. Montecucco, J. Siviter, and A. R. Knox, “Simple, Fast and Accurate Maximum Power Point Tracking Converter for Thermoelectric Generators,” in *Energy Conversion Congress and Exposition (ECCE), IEEE*, 2012, pp. 2777–2783.
[36] R.-Y. Kim and J.-S. Lai, “A Seamless Mode Transfer Maximum Power Point Tracking Controller For Thermoelectric Generator Applications,” *IEEE Trans. Power Electron.*, vol. 23, no. 5, pp. 2310–2318, 2008.
[37] D. Champier, C. Favarel, J. P. Bédécarrats, T. Kousksou, and J. F. Rozis, “Prototype Combined Heater/Thermoelectric Power Generator for Remote Applications,” *J. Electron. Mater.*, Jan. 2013.
[38] R.-Y. Kim, J.-S. Lai, B. York, and A. Koran, “Analysis and Design of Maximum Power Point Tracking Scheme for Thermoelectric Battery Energy Storage System,” *IEEE Trans. Ind. Electron.*, vol. 56, no. 9, pp. 3709–3716, Sep. 2009.
[39] A. Montecucco and A. R. Knox, “Maximum Power Point Tracking Converter Based on the Open-Circuit Voltage Method for Thermoelectric Generators,” *IEEE Trans. Power Electron.*, vol. 30, no. 2, pp. 828–839, 2015.
[40] A. Petucco, S. Saggini, L. Corradini, and P. Mattavelli, “Analysis of Power Processing Architectures for Thermoelectric Energy Harvesting,” *IEEE J. Emerg. Sel. Top. Power Electron.*, vol. 6777, no. c, pp. 1–1, 2016.
[41] E. A. Man, D. Sera, L. Mathe, E. Schaltz, and L. Rosendahl, “Dynamic Performance of Maximum Power Point Trackers in TEG Systems Under Rapidly Changing Temperature Conditions,” *J. Electron. Mater.*, vol. 45, no. 3, pp. 1309–1315, 2016.
[42] P. Dziurdzia (2011). Modeling and Simulation of Thermoelectric Energy Harvesting Processes, Sustainable Energy Harvesting Technologies - Past, Present and Future, Dr. Yen KhengTan (Ed.), ISBN: 978-953-307-438-2, InTech, Available from: http://www.intechopen.com/books/sustainable-energy-harvesting-technologies-past-present-and-future/modeling-and-simulation-of-thermoelectric-energy-harvesting-processes
[43] Thermoelectric Conversion Systems, “Testing Thermoelectric Generators”, *Application Note* n. 2901, http://www.TEconversion.com
[44] Y. Tian, B. Xia, Z. Xu, W. Sun. "Modified Asymmetrical Variable Step Size Incremental Conductance Maximum Power Point Tracking Method for Photovoltaic Systems". *Journal of Power Electronics,* Vol. 14, No. 1, pp.156-164, January 2014.
[45] J. Ahmed, Z. Salam. "An improved perturb and observe (P&O) maximum power point tracking (MPPT) algorithm for higher efficiency". *Appl. Energy* No. 150 (2015), pp. 97-108.
[46] R. Leyva, C. Olalla, H. Zazo, C. Cabal, A. Cid-Pastor, I. Queinnec, C. Alonso. "MPPT Based on Sinusoidal Extremum-Seeking Control in PV Generation". *International Journal of Photoenergy*. Volume 2012 Article ID 672765. Doi: 10.1155/2012/672665. Hindawi Publishing Corporation.
[47] R. Leyva, C. Alonso, I. Queinnec, A. Cid-Pastor, D. Lagrange, L. Martinez-Salamero. "MPPT of Photovoltaic Systems using Extremum-Seeking Control". *IEEE Transactions on Aerospace and Electronic Systems*. Vol. 42, No.1, January 2006.